Analysis of Dissimilar Welding Joint between Inconel 718 and AISI 316L by GTAW Multipass Process

Rafaela dos Santos Silva[1] ⓘ, Rudineli Demarque[2] ⓘ, Leonardo Martins da Silva[1] ⓘ, José Adilson de Castro[1] ⓘ

[1] Universidade Federal Fluminense – UFF, Programa de Pós-Graduação em Engenharia Metalúrgica, Volta Redonda, RJ, Brasil.
[2] Universidade Federal do Rio de Janeiro – UFRJ, Departamento de Engenharia Mecânica, Macaé, RJ, Brasil.

Abstract: AISI 316L steel and Inconel 718 are metals of wide application in industries. The study of dissimilar welding between these two materials is technologically important to improve their joint performance. We focused this study on the evaluation of the dissimilar weldability of these materials. Three samples of AISI 316L and Inconel 718 welded using a multipass GTAW (Gas Tungsten Arc Welding) process with different parameters were analyzed. The microstructural characterization, measurements of the volumetric fraction of the δ ferrite and Laves phase, the spacing between austenite dendrites, in addition to measurement and analysis of dimensions of the welding zones and the microhardness were performed. The measurement of the weld metal dimensions and the dendrite spacing showed that higher heat inputs increased the dilution zones and the spacing between austenite dendrites. The volumetric fraction of the δ ferrite decreased with the increase of heat input, while the Laves phase fraction increased. The microhardness presented significant variation in the weld pool due to changes in the phases and composition, as evidenced by EDS analysis in the dissimilar joints.

Key-words: Austenitic stainless steel; Superalloys; Laves phase; Multipass welding; Dissimilar welding.

Análise da Junta Soldada Dissimilar entre Inconel 718 e AISI 316L pelo Processo GTAW Multipass

Resumo: O aço AISI 316L e Inconel 718 são metais de ampla aplicação na indústria. O estudo da soldagem dissimilar entre esses dois materiais é tecnologicamente importante para melhorar o desempenho da junta. Concentramos este estudo na avaliação da soldabilidade dissimilar desses materiais. Três amostras de AISI 316L e Inconel 718 soldadas usando processo multipass GTAW (Gas Tungsten Arc Welding) com diferentes parâmetros foram analisadas. Foram realizadas caracterização microestrutural, medidas da fração volumétrica da ferrita δ e fase Laves, espaçamento entre as dendritas de austenita, além da medição e análise das dimensões do metal de solda e da microdureza. A medição das dimensões do metal de solda e do espaçamento entre as dendritas mostrou que maiores aportes térmicos aumentaram as zonas fundidas e o espaçamento entre as dendritas de austenita. A fração volumétrica de ferrita δ diminuiu com o aumento do aporte térmico, enquanto que a fração da fase Laves aumentou. A microdureza apresentou variação significativa na poça de fusão devido a mudanças nas fases e na composição, conforme evidenciado pela análise de EDS nas juntas dissimilares.

Palavras-chave: Aço inoxidável austenítico; Superligas; Fase laves; Soldagem multipasse; Soldagem dissimilar.

1. Introduction

Austenitic stainless steels can be used from cryogenic temperatures to high temperatures providing a good combination of ductility, strength, toughness and good oxidation-corrosion resistance. They have good weldability and among them, AISI 316L has lower carbon content in its composition, which promotes better weldability [1,2]. Nickel-based superalloys are often used in harsh environments, such as gas turbines and power generation [3]. The Inconel 718 superalloy is a high-cost precipitation hardened alloy with high resistance to corrosion and high temperatures, with excellent creep resistance and good oxidation resistance. Inconel 718, like some other nickel superalloys, has the addition of niobium which favors the formation of precipitates that increase the strength of the alloy and also favors the prevention of the occurrence of solidification cracks [3-6]. In summary, AISI 316L and Inconel 718 are high temperature materials that can be applied in corrosive environments. Both metals present austenitic microstructure and good weldability.

Dissimilar welding, a common practice in industries, promotes the union of two alloys with different chemical compositions. This type of welding allows adapting materials to the environment, using, for example, a lower cost material in places that do not require high mechanical and corrosion resistance. It is important to emphasize that the properties of the

dissimilar fusion zone must be equal to or greater than the properties of the weaker base metal. Besides, dissimilar welding is a method that requires proper planning of the welding parameters so that it does not affect the performance of the part in service [7]. The dissimilar welding practice between Inconel 718 and AISI 316L is common in aerospace industries and nuclear power plants. Ferretti et al. [8] reported the use of dissimilar welding between Inconel 718 connectors and AISI 316L tubes for transporting ammonia in an international space station. Henderson et al. [9] reported the use of dissimilar joints of AISI 316L and Inconel 718 in industrial gas turbine engines. Silva et al. [10] studied the corrosion resistance of dissimilar joints of Inconel 718 and AISI 316L welded by GTAW process under different heat inputs and concluded that Inconel 718 and the fusion zone (FZ) have good resistance to pitting corrosion, although in the region close to AISI 316L steel may suffer localized corrosion. Gomes et al. [11], using the Hole-Drilling technique, analyzed the presence of residual stresses in dissimilar joints of AISI 316L and Inconel 718, concluding that the interface between the base metal and heat-affected zone (HAZ) of each metal presented residual stress around 300 MPa. Using the multipass GTAW process, Ramkumar et al. [12] compared the similar welding of AISI 316L and Inconel 718 with the dissimilar welding between AISI 316L and Inconel 718 and concluded that the dissimilar joint has better tensile strength than the similar joints of both materials.

It is observed that the study of dissimilar welding between Inconel 718 and AISI 316L is of utmost industrial importance due to its use in harsh environments, and the wrong choice of welding parameters can lead to service failure. Besides, due to the Inconel 718 chemical composition and the cooling rate of the welding process, the secondary Laves phase can be formed in the FZ, which impairs the properties of the weld due to the high hardness and fragility of this phase [13]. It is noticed that in the literature, there are still scarce studies on the effects of heat input on the microstructure of dissimilar joints of Inconel 718 - AISI 316L and the formation of Laves phase in these joints. Therefore, the present study aims to characterize and evaluate the properties of dissimilar welded joints of Inconel 718 – AISI 316L welded by the multipass autogenous GTAW process, analyzing the influence of welding parameters on the microstructural and macrostructural characteristics of the weld metal and the formation of the Laves phase.

2. Materials and Methods

2.1. Material

Three AISI 316L stainless steel plates and three plates of Inconel 718 were used, both of them hot rolled. All plates had the same dimensions: 120 mm x 20 mm x 5 mm. The standard chemical composition of AISI 316L and Inconel 718 is shown in Table 1 and Table 2, respectively, and the chemical composition of the main elements of each material according to the manufacturers is shown in Table 3.

Table 1. Standard chemical composition (wt %) of AISI 316L [14].

C	Mn	P	S	Si	Cr	Ni	Mo
0.030	2.00	0.045	0.030	1.00	16.00/18.00	10.00/14.00	2.00/3.00

Table 2. Standard chemical composition (wt %) of Inconel 718 [15].

Ni	Cr	Fe	Co	Mo	Nb	Ti	Al	C	Mn	Si	Cu
50.0-55.0	17.0-21.0	Bal.	1.00	2.80-3.30	4.75-5.50	0.35	0.20-0.80	0.08	0.35	0.35	0.30

Table 3. Chemical composition (wt. %) of the main elements of AISI 316L and Inconel 718, according to the manufacturers.

Alloy	C	Cr	Ni	Si	Mn	Mo	Cu	Ti	Al	Nb	Fe
316L	0.021	17.08	10.02	0.42	1.33	2.026	0.101	-	0.0036	-	Bal.
718	0.021	18.0	52.4	0.03	0.02	2.95	0.01	0.98	0.44	4.97	20.01

2.2. Welding process

Inconel 718 and AISI 316L plates were welded in the butt joint position without bevel by an autogenous GTAW process with a welding speed of 4.5 mm s^{-1} using a multi-pass technique, with three welding passes (same current, temperature and voltage) being carried out on each sample. A 1/8" thoriated tungsten electrode with 45˚ angulation was used. Argon was the

shielding gas with a flow rate of 17 L min^{-1}. Fixed inter-pass temperature and varied current were used, as shown in Table 4, where the welding parameters are found. The inter-pass temperature and current values were established in a previous study [16], in which an experimental planning was realized following the Calegare method [17]. Knowing that the η efficiency is equal to 0.8 for the autogenous GTAW process [18], the welding heat input was calculated according to Equation 1, whose results are also shown in Table 4.

$$Heat\ Input = \frac{Voltage \times Current \times \eta}{Welding\ Speed}$$ (1) [18]

Table 4. Parameters and heat inputs of GTAW welding processes.

Test	Current (A)	Temperature (ºC)	Voltage (V)	Welding Speed (mm s^{-1})	Flow Rate Ar (L min^{-1})	Heat Input (kJ/mm)
Sample 1	160	600	12.7	4.5	17	0.361
Sample 2	180	600	13.6	4.5	17	0.435
Sample 3	200	600	15.5	4.5	17	0.551

After welding, the three plates were cut to the dimensions shown in Figure 1. For comparison purposes, an as-received sample of each material was used for characterization.
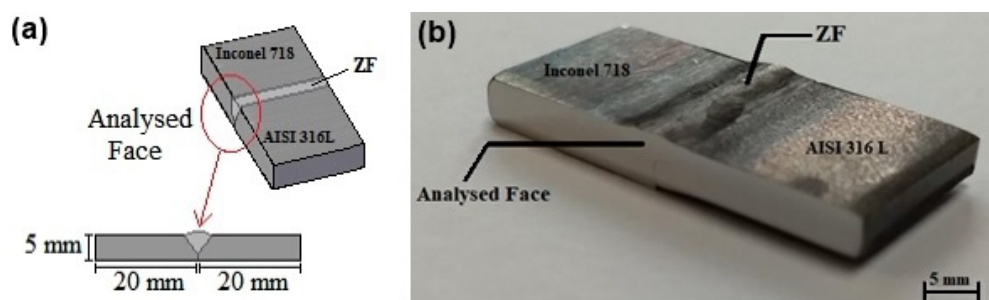

Figure 1. (a) Scheme of the samples welded by the GTAW process emphasizing the region analyzed. (b) Photograph of one of the analyzed samples.

2.3. Microstructure and macrostructure characterization

All samples, both welded and as-received, were hand-sanded in Knuth - Rotor 2 Struers using SiC sandpapers in the sequence of 220 to 4000 mesh. The polishing process was carried out in a double metallographic polishing machine, PL 02 ED, using a diamond paste of 3 μm and then 1 μm as an abrasive. For the as-received and the welded samples, the microstructure was revealed by a reagent composed of three parts of HCl 37% for one part of HNO$_3$, enabling the analysis of the presence of δ ferrite in the welded sample. In order to analyze only the Laves phase present in the welded samples, the samples were again hand-sanded and polished and this time it was used Marble reagent (4 g of CuSO4, 20 mL of HCl and 20 mL of H2O). If exposed for a short period of time, 5 seconds in the present study, Marble reagent reveals only the Laves phase and not the δ ferrite.

For as-received samples, the average grain size was calculated using the Heyn linear intercept method, according to the ASTM E112 standard [19]. The welded samples and the as-received samples were analyzed by optical microscopy (OM) and by scanning electron microscopy (SEM), which was used in two modes: scattered electron (SE) and backscattered electron (BSD). Using the ImageJ software, the quantification of δ ferrite and Laves phase was performed in ten micrographs of each welded sample to obtain the average quantification. Besides, the dendrite spacing in the fusion zone was also analyzed using ImageJ. In other words, the distance between the austenite dendrites in different areas was measured. For each sample, three micrographs of different regions of the fusion zone were used. Ten spacing measurements were made for each micrograph, totaling thirty spacing measurements between austenite dendrites for each welded sample. The Laves phase was analyzed by SE and the BSD technique was also performed to visualize the morphology of the Laves phase. As for the macrostructural analysis, the sizing of the weld bead was analyzed by measuring the width, penetration depth and area of the weld joint. The weld bead width and penetration measurements were made using a Union Optical profilometer, with each measurement

being performed twice. The measurement of the area was made using the GeoGebra software, which allows the approximate measurement of the weld bead area through the insertion of points in macrographs of the welded joint. Three micrographs obtained through a stereomicroscope using a 16X magnification were used. The dilution between Inconel 718 and AISI 316L of each welded sample was also calculated, using the Equation 2 and Figure 2.
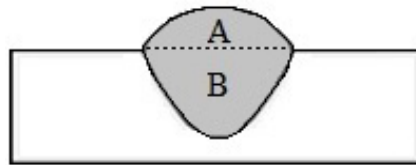
$$Dilution(\%) = \frac{B}{A+B} \times 100 \qquad\qquad (2)\ [12]$$

Figure 2. Measurement scheme for calculating the dilution.

2.4. Vickers microhardness and chemical composition analysis

Vickers microhardness tests were performed on samples as-received in ten different regions, obtaining the average hardness. As in the studies by Anawa and Olabi [20] and Yin et al. [21], the microhardness was measured in all regions of the cross-section of the welded samples, including the base metals, both HAZ and FZ, in order to evaluate the changes in microhardness in the dissimilar joint regions. The microhardness measurements were made 1 mm away from the surface, as shown in Figure 3. The distance between each measurement was 1 mm. Each test was performed using a load of 300 gram-force for 30 seconds.
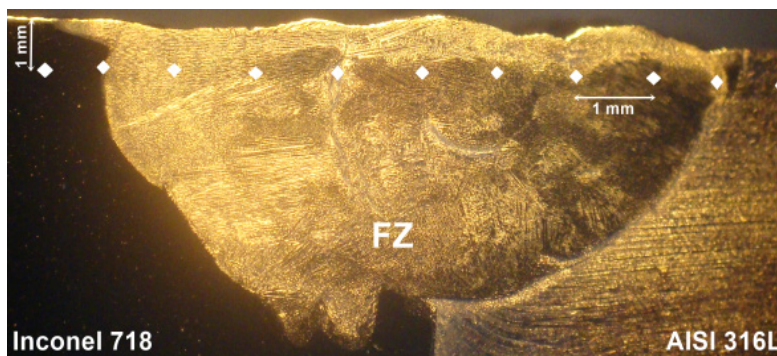

Figure 3. Scheme of the microhardness measurements of the welded samples.

The technique of energy dispersive spectroscopy (EDS) was used to analyze the chemical composition of the FZ, being measured at several random points resulting in the average of the elements present. The variation of the chemical composition in each region of the welded sample was also determined by EDS, using in-line analysis, same method used in the studies by He et al. [22], Upadhyaya and Singh [23] and Barnabas et al. [24]. The HAZ close to AISI 316L (HAZ 316L), the FZ and the HAZ close to Inconel 718 (HAZ 718) of sample 2 were analyzed, as shown in Figure 4. Only sample 2 was chosen because it was the sample welded with intermediate current and, consequently, intermediate heat input. Besides, the comparative analysis of the chemical composition of welded samples with different heat inputs is not the aim of this study. The chemical composition of the Ni and Fe present in the FZ of each sample was compared with the content calculated according with the previously calculated dilution. These elements, Ni and Fe, were chosen because they are the elements that suffer the greatest variation in the transition FZ/AISI 316L and FZ/Inconel 718. The content of Ni and Fe was calculated using Equation 3.

$$Element\ content = \frac{Content\ of\ AISI\ 316L + Content\ of\ Inconel\ 718}{2} \times Dilution(\%) \qquad (3)\ [12]$$

In addition, EDS analysis was used to evaluate the chemical composition of the Laves phase. In this case, it was used punctual EDS analysis, and several points of the Laves phase present in sample 3 were measured. As the intention was just to analyze the chemical composition of the Laves phase, only one sample (sample 3) was chosen for EDS analysis.
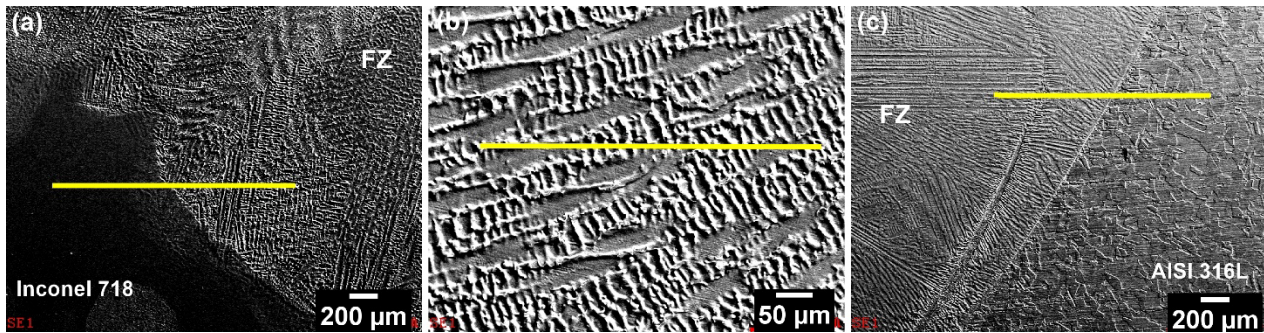
Figure 4. EDS path analysis performed on sample 2. (a) analysis of HAZ 718. (b) analysis of the FZ. (c) analysis of HAZ 316L.

3. Results and Discussion

3.1. Analysis of samples as-received

Figure 5 shows the microstructure of AISI 316L and Inconel718, respectively. It is observed, for both samples, the presence of twin boundaries, possibly formed during the hot rolled process. The micrograph also shows the different grain sizes in both materials. The average grain size was 64 ± 7 µm for Inconel 718 and 31 ± 2 µm for AISI 316L. The result of the ASTM E-112 grain size was 5 for Inconel 718 and 7 for AISI 316L steel. The microhardness test resulted in 237 ± 1 HV for Inconel 718 and 169 ± 0.50 HV for AISI 316L.
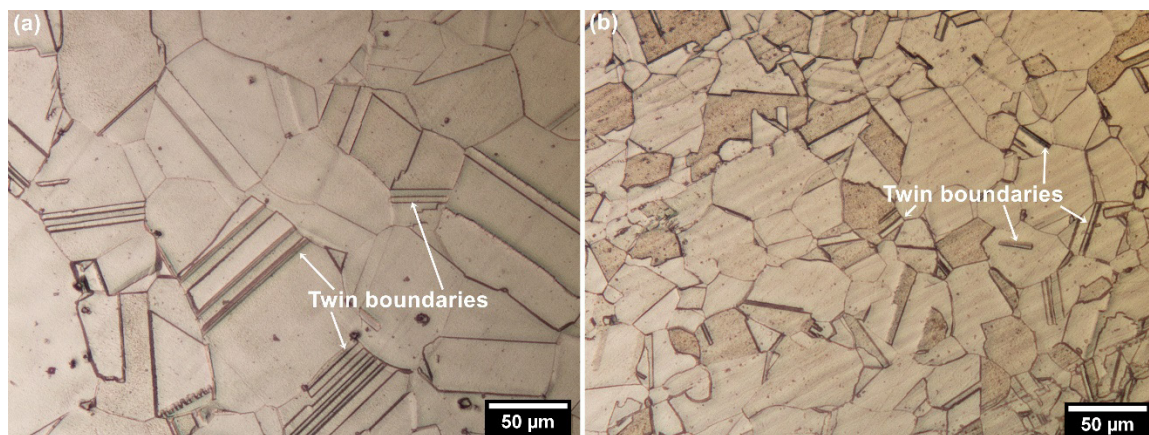

Figure 5. The microstructure of the alloys. (a) Inconel 718. (b) AISI 316L.

3.2. Analysis of welded samples

Figure 6 shows macrographs of each welded samples with the markings used to measure the width, penetration depth and area of the weld joint. The results of the dimensioning of the welded samples are shown in Figure 7. As observed by Royse [25] and Demarque et al. [16], the weld bead dimensions increase with increasing heat input since higher heat inputs imply a higher amount of energy transferred to the metal, resulting in a greater weld pool, as shown in the graph results. It can be observed that the increase in the penetration of sample 3 (greater heat input) in relation to the penetration of sample 1 (lower heat input) was 6.2%, while the increase in the width of sample 3 in relation to the width of sample 1 was 49.6%, in other words, the increase in the width of the weld bead in relation to the heat input was more significant. Sample 1 showed very low penetration compared to samples 2 and 3. It is important to emphasize that the low penetration depth can lead to defects in the weld root, leading to failure in service. It is interesting to note that sample 2 showed greater penetration than sample 3. However, sample 2 presented a smaller width than sample 3 and also than sample 1 (7.6% smaller than sample 3 and 1.5% smaller than sample 1). The fact that sample 2 presented greater penetration and smaller width than samples 1 and 3 can be explained by a preferential dissipation of welding energy in the normal direction (resulting in a higher penetration), and not in the transverse direction (resulting in a smaller width). This may have occurred due to the action of an external magnetic field that distorted the welding arc, redirecting the heat flow, or it could have occurred due to some heterogeneity of the thermophysical properties of the materials between these two directions (normal x transverse).

Therefore, the area of sample 2 remained larger than the area of sample 1 and smaller than the area of sample 3, as expected due to its heat input.

The results of the calculated dilution were 86.85% for sample 1, 92.59% for sample 2 and 91.94% for sample 3, as it can be seen in Figure 7. It was expected that samples 2 and 3 had a greater dilution than sample 1, as they were welded with higher heat input. The fact that sample 2 had a higher dilution than sample 3 may be related to this sample having presented greater penetration than the others.
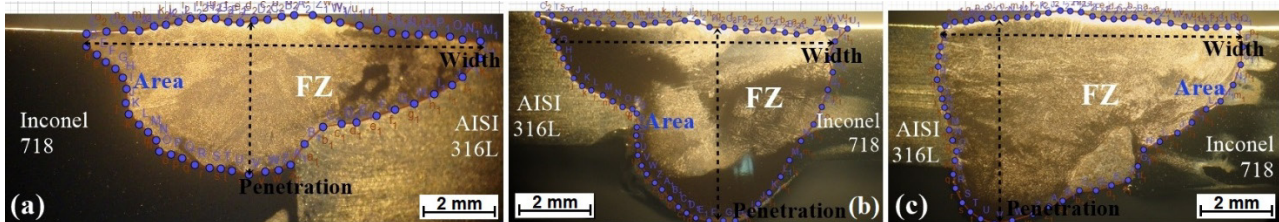

Figure 6. Macroscopy of the welded samples: (a) Sample 1. (b) Sample 2. (c) Sample 3.
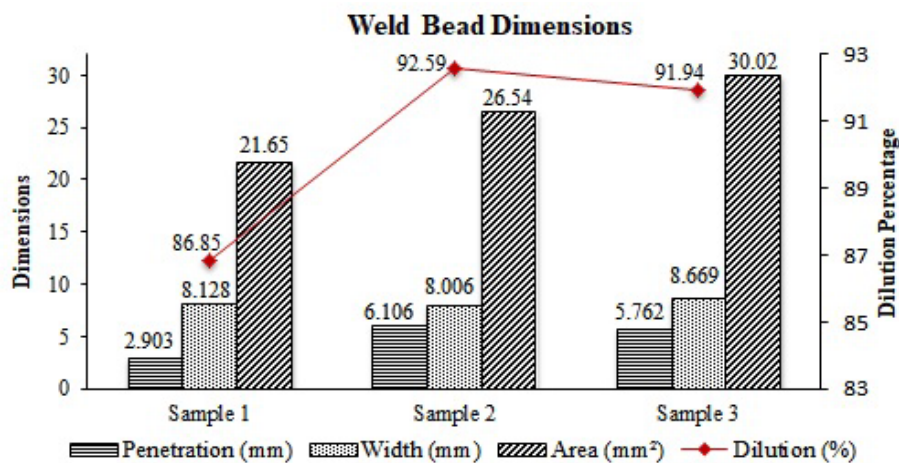

Figure 7. Weld bead dimensions and dilution percentage of each sample.

Figures 8, 9 and 10 show the microstructures of the FZ, HAZ 718 and HAZ 316L of each welded sample. The FZ of all the studied samples consists of austenite dendrites with δ ferrite present mainly in the austenite contours. This microstructure was already expected since, according to Lippold and Kotecki [26], during the solidification of AISI 316L, δ ferrite formation occurs in the form of dendrites with the later formation of austenite, which consumes part of the ferrite, which can be skeletal ferrite or lathy ferrite (FA solidification). Figure 11 shows an adapted diagram that illustrates the formation of δ ferrite in AISI 316L steel [26,27] and Figure 12 shows the Schaeffler diagram for the solidification of AISI 316L. It is possible to observe that, according to the composition of AISI 316L, the microstructure of the welded stainless steel consists of austenite and approximately 10% δ ferrite. Therefore, in dissimilar welding of this material, this type of solidification was expected to occur, with the presence of δ ferrite in the interdendritic region. Despite that Figure 11 shows a predominance of lathy ferrite in AISI 316L, in dissimilar welding, there is a predominance of skeletal ferrite, as can be observed in Figures 8a, 9a and 10a. The formation of predominantly columnar austenite dendrites with the formation of cellular dendrites was also expected, as the dendritic microstructure is typical of solidification after the welding process due to the cooling rate, which can be explained by the supercooling constitutional theory developed by Rutter and Chalmers [28] and later explained by Kou [29]. In the OM analysis, it is not possible to observe clearly; however, in the SEM analysis (to be shown in Figure 13), the formation of the Laves phase in the interdendritic region is clear.

Observing the FZ of each sample, it is possible to visually perceive that higher heat inputs from welding result in greater dendrite spacing. The quantitative result is shown in Table 5. It is possible to observe the microstructural difference between the FZ, HAZ 718 and HAZ 316L. The HAZ region reaches a lower temperature during welding and is exposed to it for a shorter time than the FZ, besides, it is a region that does not melt. Therefore, during welding, HAZ undergoes fewer microstructural changes than the FZ, as shown in the Figures 8, 9 and 10. It is also possible to observe that HAZ 718 is different from HAZ 316L.

Both materials, AISI 316L and Inconel 718, have different chemical composition and different thermophysical properties, which contributes to the microstructural change to be different.
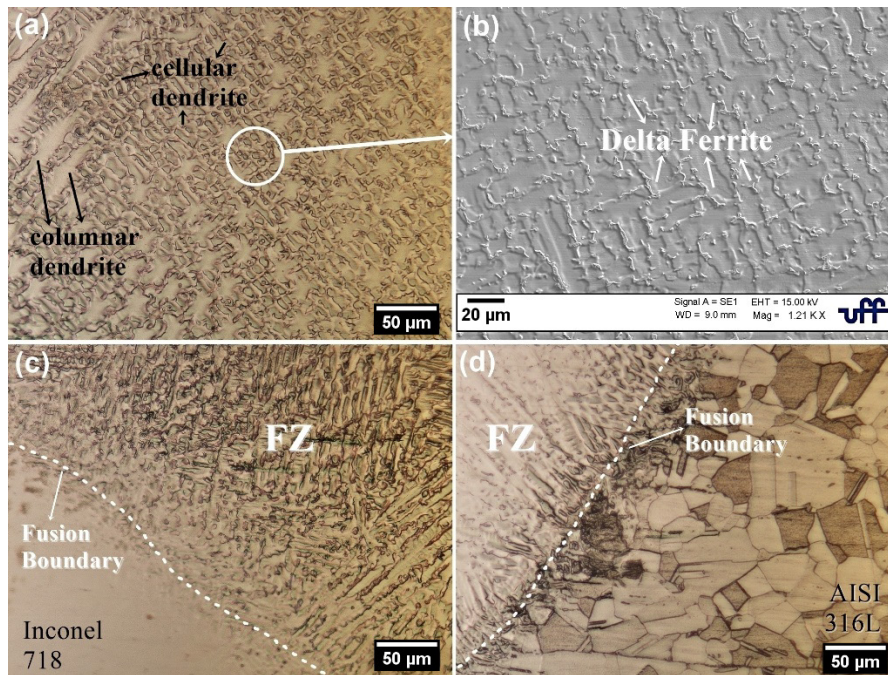

Figure 8. Micrographs of sample 1. (a) FZ, OM 200X. (b) FZ with higher magnification (1210X), image obtained by SEM. (c) HAZ 718, OM 200X. (d) HAZ 316L, OM 200X.
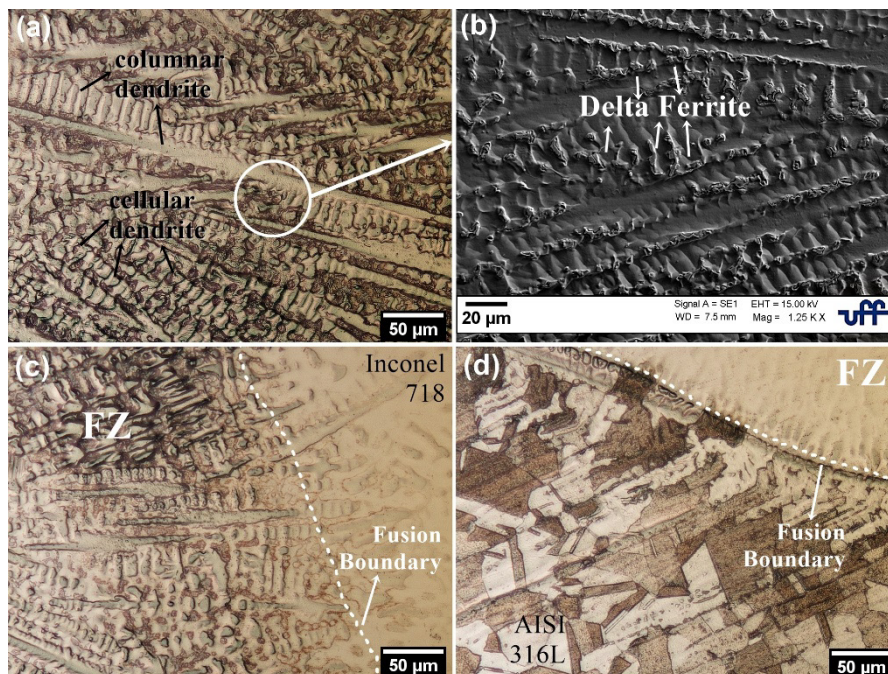

Figure 9. Micrographs of sample 2. (a) FZ, OM 200X. (b) FZ with higher magnification (1250X), image obtained by SEM. (c) HAZ 718, OM 200X. (d) HAZ 316L, OM 200X.
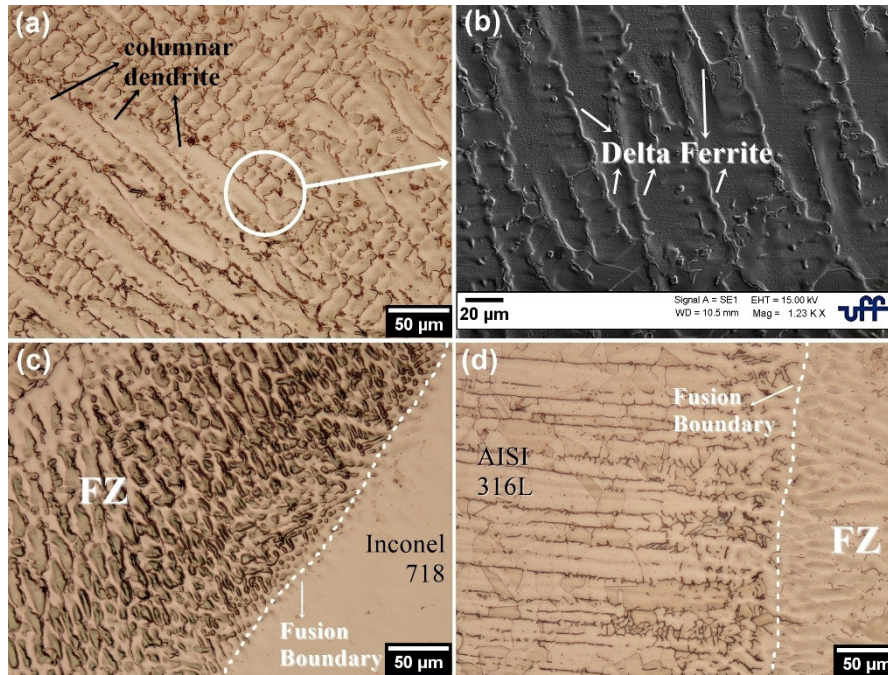
Figure 10. Micrographs of sample 3. (a) FZ, OM 200X. (b) FZ with higher magnification (1230X), image obtained by SEM. (c) HAZ 718, OM 200X. (d) HAZ 316L, OM 200X.
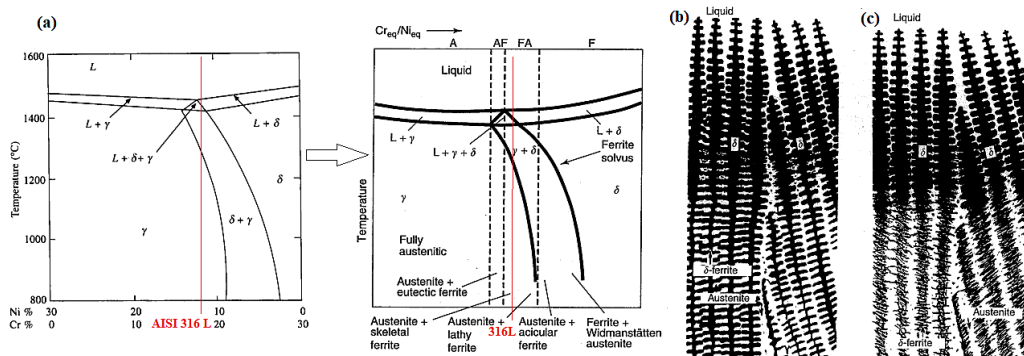

Figure 11. (a) Solidification of AISI 316L steel according to chemical composition. (b) FA solidification: skeletal ferrite. (c) FA solidification: lathy ferrite. Adapted from Lippold and Kotecki [26] and Khatak and Raj [27].
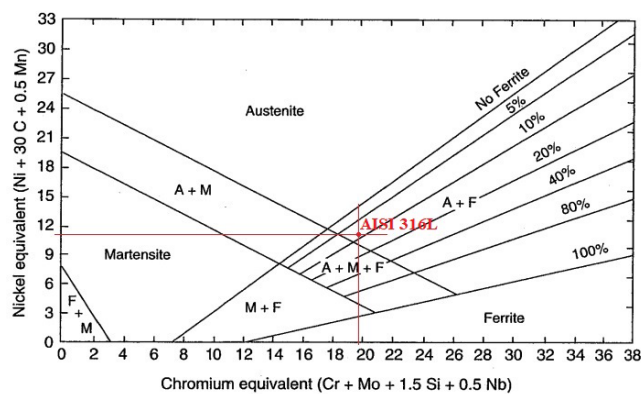

Figure 12. Schaeffler diagram for AISI 316L. Adapted from Lippold and Kotecki [26].

Figure 13 shows the results of the SE and BSD analyzes focusing on the Laves phase. Figure 13a shows that the Laves phase forms in the interdendritic region, where there was the formation of δ ferrite. Figure 13a also shows that, as studied by Sohrabi et al. [13], what is known as the Laves phase is actually an eutectic constituent formed by Laves and austenite and nucleate on δ ferrite. The BSD analysis, Figure 13b, shows the different phases found in the FZ microstructure through the difference in shades: black represents austenite, dark gray represents δ ferrite and light gray represents Laves. The microstructural images (Figure 13) indicate the presence of Laves phase close to the δ ferrite. Based on the literature [13], the Laves phase has a tendency to form close to the δ ferrite, as shown in Figure 13, since the δ ferrite is present in the dendrite boundaries and the dendrite boundaries are regions with a tendency to form the Laves phase.
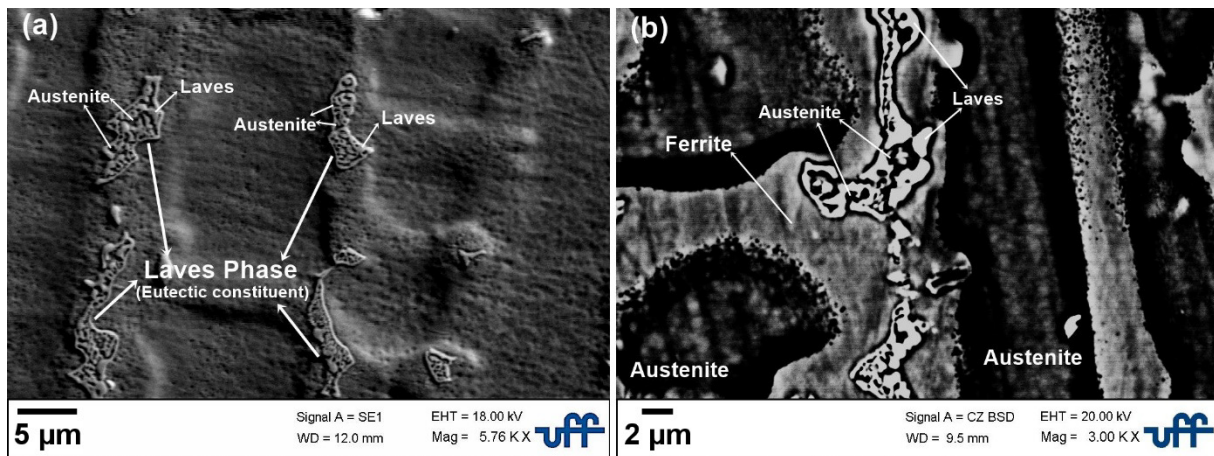

Figure 13. Laves phase present in sample 2. (a) Microscopy of the Laves phase through SEM analysis. (b) BSD analysis shows a eutectic constituent formed from Laves and austenite, present on δ ferrites.

Figures 14a and 15a show one of the micrographs used to analyze the volume fraction of δ ferrite and Laves phase, respectively. Figures 14b and 15b show the processed micrograph obtained by the software ImageJ as a way to quantify the volume fraction of the δ ferrite and Laves phase, respectively. As explained in item 2.3, in order to analyze δ ferrite and Laves phase separately, the samples were exposed by two different reagents to avoid confusing the phases.

It is possible to observe in Tables 5 and 6, respectively, the results obtained from the quantification of δ ferrite and Laves phase in the FZ and the dendrite spacing with a 95% confidence interval. The volumetric fraction of δ ferrite, shown in Table 5, is higher than predicted in the Schaeffler diagram. As can be observed, the higher the heat input applied during the welding process, the lower the volumetric fraction of δ ferrite and the higher the spacing between austenite dendrites. According to Kou [29], the heat input affects the thermal cycle, because the higher the heat input, the slower the cooling rate and there will be more time for the nucleation and growth of the austenite dendrites. This increases the dendrite spacing and decreases the δ ferrite fraction since, according to Lippold and Kotecki [26], the austenite that forms during solidification consumes part of the ferrite. A study developed by Silva et al. [30] had already shown that when welding AISI 316L steel using the autogenous GTAW method, the dendrite spacing increases according to the increase in heat input. In this study, it is observed that the same is valid for dissimilar welding. Observing Table 5, it is also noted that the volumetric fraction of Laves phase increases with the increase of heat input. As explained above, the higher the heat input, the higher the amount of energy transferred to the weld and the slower the cooling rate, consequently, there will be more time for the nucleation and growth of the Laves phase. Furthermore, the iron content in the solidified zone reduces the equilibrium partition coefficient (k) of niobium and molybdenum, increasing the Laves phase content. Thus, in order to reduce the Laves phase formation during welding involving Inconel 718, it is recommended to use low weld heat inputs [31]. The Laves phase is a deleterious phase that can negatively alter the mechanical properties of the material [13]. Sohrabi et al. [13] and Miao et al. [32] found respectively 3.57% and 3.2% of the amount of the as cast Laves phase present in the Inconel 718. Comparing with Table 5, it is observed that the amount of Laves phase found in the present study is high. According to Sohrabi et al. [13], the amount of Laves phase is dependent on the Nb content and cooling rate, which may explain the large volume fraction formed during welding in this study. Despite the amount of the fragile Laves phase in the FZ, there was no weld crack evidence. In Figure 16 it is possible to see clearly that when the heat input increases, the volumetric fraction of Laves phase also increases and the volumetric fraction of δ ferrite decreases.
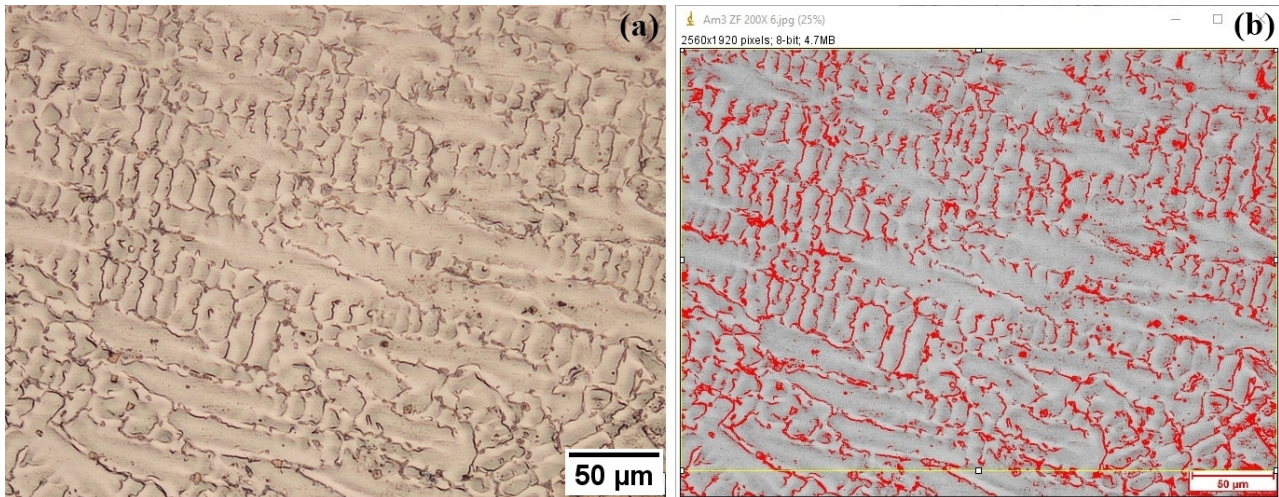
Figure 14. (a) δ ferrite in the microstructure. (b) Processed micrograph of (a) in the ImageJ.
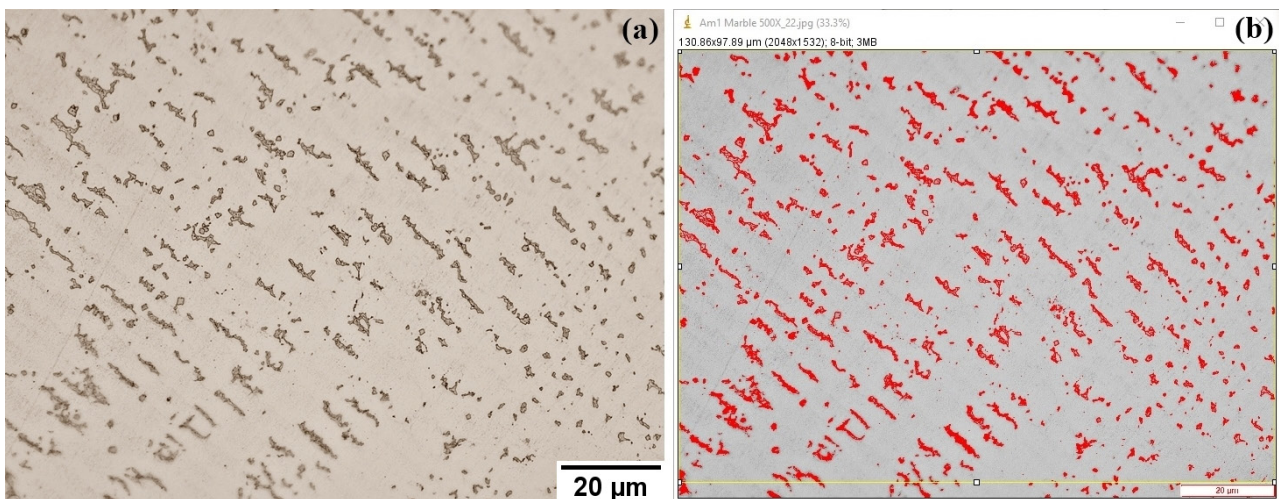

Figure 15. (a) Laves phase in the microstructure. (b) Processed micrograph of (a) in the ImageJ.

Table 5. The volumetric fraction of δ ferrite and Laves phase of the welded samples.

	δ Ferrite (wt. %)	Laves (wt. %)
Sample 1	(15.02±0.72)	(6.77±0.11)
Sample 2	(13.54±0.75)	(7.80±0.16)
Sample 3	(10.73±0.61)	(8.35±0.16)

Table 6. Dendrite spacing of the welded samples.

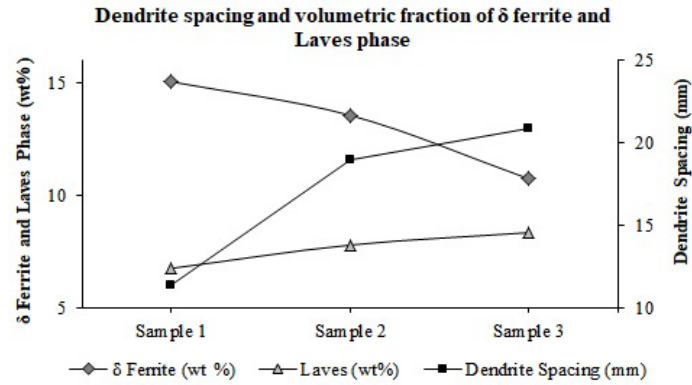|	Sample 1	Sample 2	Sample 3
Spacing length (mm)	11.376 ± 0.365	18.991 ± 0.441	20.880 ± 0.727

Figure 16. Graph showing the volumetric fraction of δ ferrite and Laves phase and the dendrite spacing of each sample.

3.3. Vickers microhardness and chemical composition analysis

The results of the microhardness profile are shown in the graph in Figure 17. It is possible to notice that the microhardness values in the FZ are between the microhardness values of the AISI 316L and Inconel 718 due to the mixture of the two materials during welding. It is also noted that there is variability in the results of each sample. This is because the measurements are done on a micrometric scale. Thus, as Pessanha [33] observed, during the test, the indenter can reach regions with a predominance of austenite and regions with a predominance of δ ferrite and Laves phase, which explains the variations in the microhardness of the FZ.
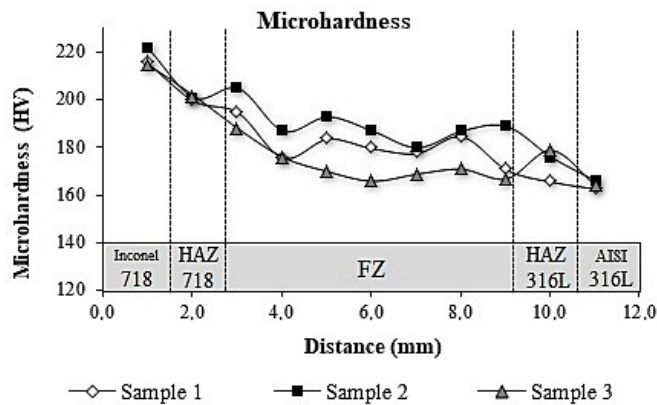

Figure 17. Results of the microhardness measurement of each sample.

Table 7 shows the chemical composition of some of the elements present on the FZ of each sample. As can be observed, not all the elements were detected by EDS, which can be explained by the similarity in wavelength and consequent misidentification of the elements. Comparing table 7 with table 5, it is observed that the higher the Nb content, the higher the volumetric fraction of the Laves phase, since the Laves phase is composed of Ni_2Nb [13].

Table 7. Chemical composition of some of the elements present in the FZ of each sample.

	Cr	Ni	Si	Mo	Al	Nb	Fe
Sample 1	16.33	30.19	0.79	2.48	0.92	4.30	36.87
Sample 2	18.83	32.62	0.80	2.49	0.95	4.13	38.80
Sample 3	16.35	29.82	0.82	not detected	0.96	4.21	36.63

Figure 18 illustrates the results of the EDS analysis for sample 2, the sample with intermediate heat input. The graphs show the variation of the chemical composition in each region (AISI 316L – HAZ 316L – FZ – HAZ 718 – Inconel 718) of the

dissimilar joint considering the three main elements present in both metals: iron, nickel and chromium. It was decided to present the chemical composition analysis through the cross-section of the sample with intermediate heat input to indicate the tendency of diffusion of one material into the other through the HAZ and FZ, showing the ascending or descending slope shape of the chemical elements. It is interesting to observe in Figure 18a that in the transition zone of FZ / HAZ 718 there is an increase in nickel content (ascending slope shape) and a decrease in iron content (descending slope shape), which was expected since the FZ is a mixture of the two welded materials and Inconel 718 has a higher content nickel and lower iron content than AISI 316L and, logically, the FZ. The reverse logic occurs in the HAZ 316L / FZ, as shown in Figure 18b. As the chromium content of AISI 316L and Inconel 718 are close, there is no significant variation in each region. Although Figure 18c shows that there is no significant variation in the elements content of the FZ, the graph presents a wave shape. This shape is due to the different phases present in the FZ (austenite, δ ferrite and Laves phase) each with different chemical composition.
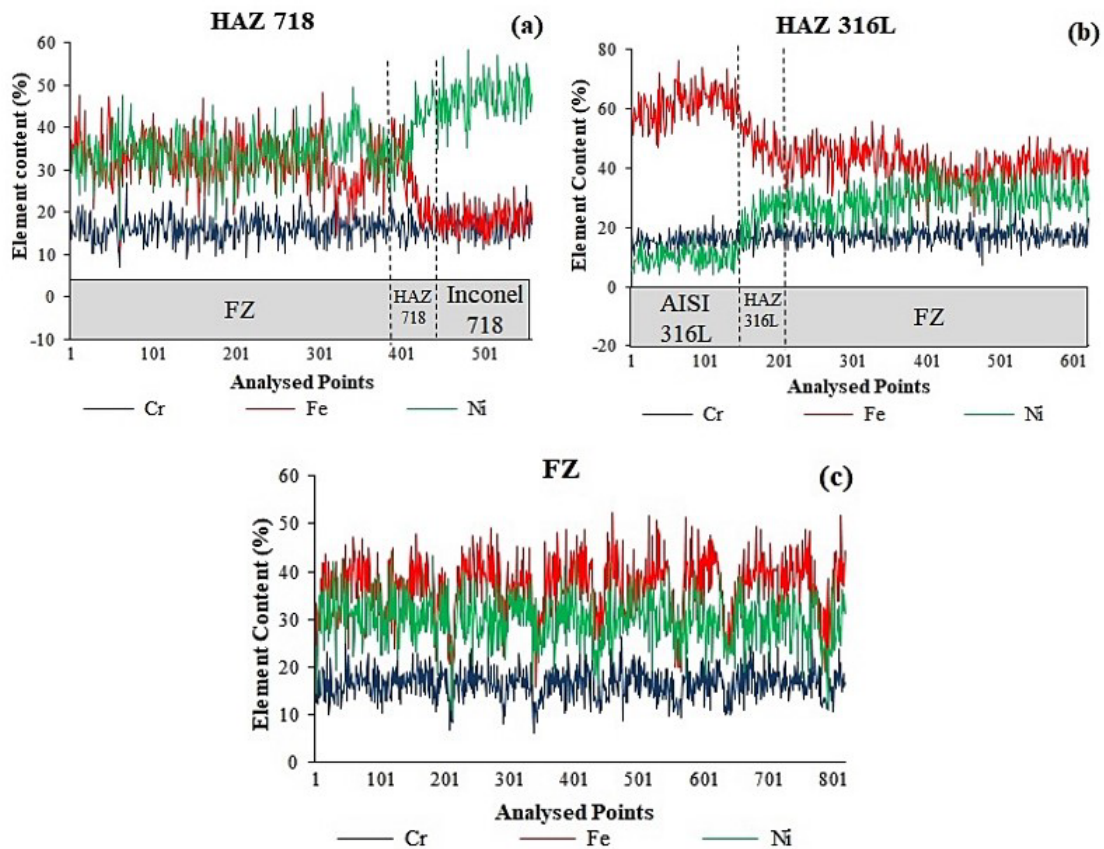

Figure 18. The main alloy elements (Fe, Ni and Cr) in sample 2. a) HAZ 718. b) HAZ 316L. c) FZ.

Table 8 shows the content of Ni and Fe of each sample according to the dilution percentage shown in Figure 16. Comparing with the experimental content shown in Table 7, it is possible to observe that the calculated and experimental contents of Ni and Fe are relatively close.

Table 8. Calculated content of Ni and Fe according with the dilution percentage.

	Sample 1	Sample 2	Sample 3
Ni	27.11	28.90	28.70
Fe	38.65	41.20	40.91

Figure 19 shows the result of the EDS analysis of the Laves phase present in sample 3. As can be seen in Figure 11, the Laves phase is actually a eutectic constituent of Laves and austenite. Nonetheless, in the present study, the EDS analysis was

performed considering the eutectic constituent as a whole and not Laves and austenite separately. Compared with Figure 18, it is observed that the Laves phase has lower levels of iron and chromium, with no change in nickel content. Besides, this phase has a significant content of niobium, as it can be seen in Figure 19b and Table 9. Table 9 shows the average of the analysis results with a 95% confidence interval, considering the main elements present in Laves phase: niobium, iron, nickel and chromium. The results found are close to the results found in the Laves phase study developed by Sohrabi et al. [34], especially for the content of Nb and Cr.
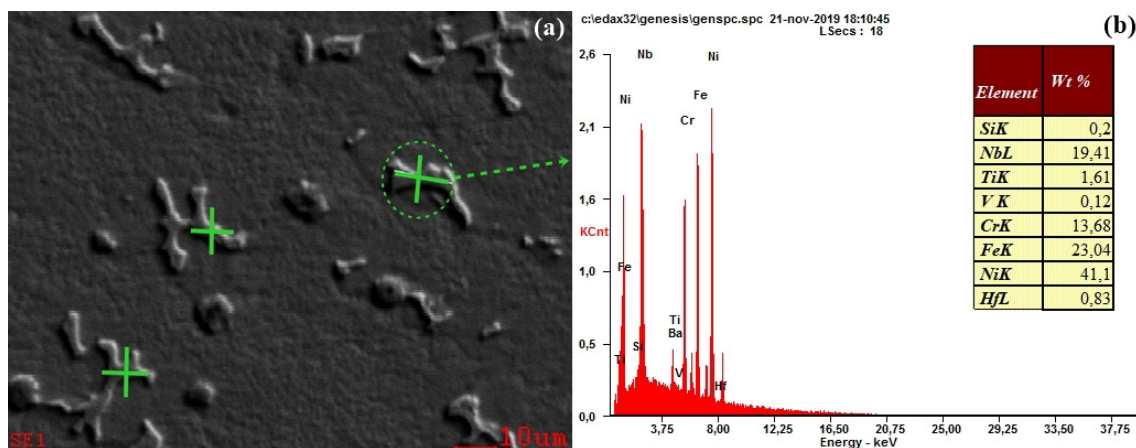

Figure 19. (a) Example of some of the punctual EDS analysis of the sample 3. (b) Result of the EDS analysis of the Laves phase made in a single point.

Table 9. Result of the EDS analysis of the Laves phase of sample 3, considering the main elements.

	Nb (wt. %)	Ni (wt. %)	Fe (wt. %)	Cr (wt. %)
Average	(18.54±1.11)	(39.38±1.76)	(22.31±1.37)	(13.18±0.78)

4. Conclusions

The main conclusions of this study are:

- The increase in heat input resulted in a lower volumetric fraction of δ ferrite, a higher fraction of the Laves phase, and greater dendrite spacing;

- It was observed that in all samples the microstructure of the fusion zone consists of austenite with the presence of columnar or cellular ferrite, and the dendrite shape varies with the increase in heat input;

- The volume fraction of Laves phase of all samples was high. Despite this, there was no weld crack evidence;

- It was observed that a larger heat input implied a larger weld pool, with sample 3 showing an increase of approximately 30% of the weld bead area in relation to sample 1;

- Due to the low penetration of sample 1, for industrial application, taking into account only the weld width and penetration, samples 2 and 3 would be more suitable;

- Sample 2 showed greater penetration and smaller width than samples 1 and 3, which was not expected. As sample 2 achieved a greater penetration even being welded with lower heat input, in industrial application, this sample would be more suitable. However, the fact that the penetration of sample 2 was greater may have been just an isolated case;

- The Vickers microhardness profile showed that there is considerable variation in the results across the regions of the welded sample, regardless of the heat input;

- The EDS analysis showed that in the FZ there is a mixture of the composition due to the fusion process of the two materials and all samples showed a dilution above 85%. There was a slope shape in the content of the elements presented according to the change in the region;

- None of the welded samples showed fracture or other defects in the weld bead. Some showed particularities, such as the low penetration of sample 1 and the high penetration of sample 2. As all samples had a high amount of Laves phase, it is

possible that the continuous use in industrial application could lead to fracture. Therefore, for practical application, a heat treatment would be indicated to reduce the amount of Laves phase in the microstructure of the samples.

Acknowledgements

References

[1] Byun TS, Garrison BE, McAlister MR, Chen X, Gussev MN, Lach TG, et al. Mechanical behavior of additively manufactured and wrought 316L stainless steels before and after neutron irradiation. J Nucl Mater. 2021;548:152849. http://dx.doi.org/10.1016/j.jnucmat.2021.152849.

[2] McGuire MF. Stainless steels for design engineers. Materials Park: ASM International; 2008. http://dx.doi.org/10.31399/asm.tb.ssde.t52310069.

[3] Akca E, Gürsel A. A review on superalloys and IN718 nickel-based Inconel superalloy. Periodicals of Engineering and Natural Sciences. 2015;3(1):15-27. http://dx.doi.org/10.21533/pen.v3i1.43.

[4] Sui S, Chen J, Zhang R, Ming X, Liu F, Lin X. The tensile deformation behavior of laser repaired Inconel 718 with a nonuniform microstructure. Materials Science and Engineering A. 2017;688:480-487. http://dx.doi.org/10.1016/j.msea.2017.01.110.

[5] Wang H, Wang L, Cui R, Wang B, Luo L, Su Y. Differences in microstructure and nano-hardness of selective laser melted Inconel 718 single tracks under various melting modes of molten pool. Journal of Materials Science and Technology. 2020;9(5):10401-10410. http://dx.doi.org/10.1016/j.jmrt.2020.07.029.

[6] Caron JL, Sowards JW. Weldability of nickel-base alloys. Comprehensive Material Processing Technology. 2014;6:151-179. http://dx.doi.org/10.1016/B978-0-08-096532-1.00615-4.

[7] Avery RE. Pay attention to dissimilar-metal welds: guidelines for welding dissimilar metals. Toronto, Canada: Nickel Development Institute, American Institute of Chemical Engineers; 1991.

[8] Ferretti S, Valenzano G, Cugno W. International space station external active thermal control system lines manufacturing. In: 57th International Astronautical Congress, 2006 May 02-06, Valencia: Spain. 2012.

[9] Henderson MB, Arrell D, Larsson R, Heobel M, Marchant G. Nickel-based superalloy welding practices for industrial gas turbine applications. Science and Technology of Welding and Joining. 2013;9(1):13-21. http://dx.doi.org/10.1179/136217104225017099.

[10] Silva GM, Ferreira EA, Castro JA. Resistência à corrosão de juntas dissimilares dos aços AISI 316L e da liga Inconel 718. Soldagem e Inspeção. 2019;24:e2422. http://dx.doi.org/10.1590/0104-9224/si24.22.

[11] Gomes DA, Castro JA, Xavier CR, Lima CAC. Analysis of residual stress by the hole-drilling method and hardness in dissimilar joints of austenitic stainless steel AISI 316L and inconel 718 alloy by autogenous GTAW process. Materials Research. 2019;22(Suppl 1):e20180844. http://dx.doi.org/10.1590/1980-5373-mr-2018-0844.

[12] Ramkumar T, Selvakumar M, Narayanasamy P, Begam AA, Mathavan P, Raj AA. Studies on the structural property, mechanical relationships and corrosion behavior of Inconel 718 and SS 316L dissimilar joints by TIG welding without using activated flux. Journal of Manufacturing Processes. 2017;30:290-298. http://dx.doi.org/10.1016/j.jmapro.2017.09.028.

[13] Sohrabi MJ, Mirzadeh H, Rafiei M. Solidification behavior and Laves phase dissolution during homogenization heat treatment of Inconel 718 superalloy. Vacuum. 2018b;154:235-243. http://dx.doi.org/10.1016/j.vacuum.2018.05.019.

[14] American Iron and Steel Institute. Welding of stainless steels and other joining methods. Toronto: Nickel Development Institute; 1998.

[15] Davis JR. Nickel, cobalt and their alloys. Materials Park: ASM International; 2000.

[16] Demarque R, Silva RS, Santos EP, Castro JA. Avaliação de parâmetros de soldagem nas características de juntas dissimilares Inconel 718-Inox 316L soldadas pelo processo TIG autógeno. Soldagem e Inspeção. 2018;23(3):380-392. http://dx.doi.org/10.1590/0104-9224/si2303.07.

[17] Calegare AJA. Introdução ao delineamento de experimentos. 2. ed. São Paulo: Blucher; 2009.

[18] Modenesi PJ, Marques PV, Santos DB. Introdução à metalurgia da soldagem. Belo Horizonte: Universidade Federal de Minas Gerais; 2012. 209 p.

[19] American Society for Testing and Materials. ASTM E112-13: Standard Test Methods for Determining Average Grain Size. West Conshohocken: ASTM International; 2013.

[20] Anawa EM, Olabi AG. Study the microhardness and microstructure of dissimilar jointed materials. In: International Conference on Microstructure and Materials Properties, Vancouver, Canada. 2014.

[21] Yin H, Gao Y, Gu Y. Evolution of the microstructure and microhardness of the welding joint of IN 740H alloy with IN 617 as filler metal. Materials Characterization. 2017;127:288-295. http://dx.doi.org/10.1016/j.matchar.2017.01.011.

[22] He Z, Cheng HN, Olanya OM, Uknalis J, Zhang X, Koplitz BD, et al. Surface characterization of cottonseed meal products by SEM, SEMEDS, XRD and XPS analysis. Journal of Materials Science Research. 2018;7(1):28-40. http://dx.doi.org/10.5539/jmsr.v7n1p28.

[23] Upadhyaya R, Singh KK. Structure property correlation of thin wall ductile iron. Journal of Materials Science Research. 2018;8(1):1-9. http://dx.doi.org/10.5539/jmsr.v8n1p1.

[24] Barnabas AA, Oyetunji A, Seidu SO. Microstructural characterization of antimony modified carbidic austempered ductile iron. Journal of Materials Science Research. 2019;8(2):36-48. http://dx.doi.org/10.5539/jmsr.v8n2p36.

[25] Royse FS. Estudo das propriedades mecânicas e microestruturais de revestimento de liga de cobalto utilizando o processo de soldagem GTAW [dissertação de mestrado]. Rio de Janeiro: CEFET-RJ; 2011. 129 p.

[26] Lippold JC, Kotecki DJ. Welding metallurgy and weldability of stainless steels. Hoboken: Wiley; 2005. 376 p.

[27] Khatak H, Raj B. Corrosion of austenitic stainless steels: mechanism, mitigation and monitoring. Burlington: Elsevier; 2002. http://dx.doi.org/10.1533/9780857094018.

[28] Rutter JW, Chalmers B. A prismatic substructure formed during the solidification of metals. Canadian Journal of Physics. 1953;31(1):15-39. http://dx.doi.org/10.1139/p53-003.

[29] Kou S. Welding metallurgy. 2. ed. New Jersey: Wiley; 2003.

[30] Silva RS, Demarque R, Santos EP, Castro JA. Influência do aporte térmico sobre as características e propriedades de cordões de solda dos aços AISI 316 e AISI 316L. Soldagem e Inspeção. 2020;25:e2504. http://dx.doi.org/10.1590/0104-9224/si25.04.

[31] Ramkumar KD, Patel SD, Praveen SS, Choudhury DJ, Prabaharan P, Arivazhagan N, et al. Influence of filler metals and welding techniques on the structure–property relationships of Inconel 718 and AISI 316L dissimilar weldments. Materials & Design. 2014;62:175-188. http://dx.doi.org/10.1016/j.matdes.2014.05.019.

[32] Miao Z, Shan A, Wu Y, Lu J, Xu W, Song H. Quantitative analysis of homogenization treatment of Inconel718 superalloy. Transactions of Nonferrous Metals Society of China. 2011;21(5):1009-1017. http://dx.doi.org/10.1016/S1003-6326(11)60814-5.

[33] Pessanha EC. Quantificação da ferrita delta e avaliação da relação microestrutura/ propriedades de um aço inoxidável austenítico 347 soldado [dissertação de mestrado]. Campos dos Goytacazes: Universidade Estadual do Norte Fluminense; 2011. 95 p.

[34] Sohrabi MJ, Mirzadeh H, Rafiei M. On the removal of Laves phase in Inconel 718 superalloy. In: Science, Technology and Knowledge: STK Conference; Hanôver, Germany. The Netherlands: CWTS; 2018.